CMS Internal Note

The content of this note is intended for CMS internal use and distribution only

22 September 2021

Study of lifetimes and cross sections of a dark vector boson with a final state of muons and dark fermions at $\sqrt{s} = 13$ TeV

Tamer Elkafrawy, Mehdi Rahmani, Marcus Hohlmann

Abstract

The maximal lifetime of a dark long-lived vector mediator with s-channel exchange is investigated analytically for a simplified model as a function of the free parameters of coupling strengths of the mediator to quarks and dark fermions as well as the mediator and dark-fermion masses. We focus on processes for which the dark vector boson couples directly to quarks and then decays to two unstable dark fermions and subsequently to the final state of two dimuons and two dark fermions. Using scaling we study the generator-level cross sections and using Monte Carlo simulation for Run 2 of the Large Hadron Collider we calculate production cross sections of the dark vector boson. Lorentz boost of lifetime for light masses of the dark vector boson is also investigated.

1 Introduction

The Standard Model (SM) of particle physics is a mathematically tight theory that describes fundamental physics and provides high-precision predictions consistent with decades of experimental studies. Nonetheless, there are several shortcomings that are of our primary interest such as the fact that the SM offers no explanation for the existence of dark matter (DM) for which there is abundant astronomical evidence [1, 2].

DM has not been measured yet, and there is not yet any direct evidence for non-gravitational interactions between DM and SM particles. DM particles do not produce direct signals in the detectors of Large Hadron Collider (LHC). However, one way to observe them might be when they are produced and decay via a visible SM particle through a spin-1 dark mediator, i.e. a dark vector boson, often called *dark vector boson* or *dark Z Z_D* that interacts with both SM and DM sectors [3, 4].

DM particles may have lifetimes that produce secondary decay vertices in collider experiments that are substantially displaced from the primary interaction vertex. We have prepared a model for dark fermions ($pp \rightarrow Z_D \rightarrow f_{D_1}\overline{f_{D_1}} \rightarrow f_{D_2}\overline{f_{D_2}}\,\mu^+\mu^-\mu^+\mu^-$), indicated in Fig. 1 as a reference model for searches for long-lived (LL) DM particles within the Compact Muon Solenoid (CMS) detector at the LHC. This model is of interest because the branching factor (B) of direct Z_D decays into dark fermions can be substantially larger than that into SM particles. This study discusses model implementation and parameterization of the vertices in the tree-level Feynman diagram with the application of Monte Carlo (MC) simulation using the framework of MADGRAPH5_aMC@NLO v2.7.0 at leading order and the model addressed in Ref. [5].
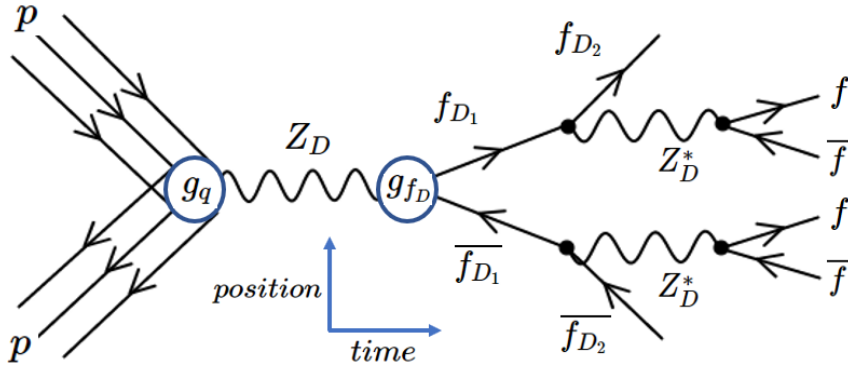
Figure 1: On-shell Z_D produced in $q\bar{q}$ interaction in pp collisions and decaying into two unstable dark fermions, which in turn decay into the final state of two lighter dark fermions and two pairs of SM fermions $f\bar{f}$ via off-shell Z_D's.

2 Vector and axial-vector couplings of the dark vector boson

The SM can be extended by adding a gauge symmetry group $U(1)$, which allows to include charged DM particles in our implemented DM model. In Fig. 1, f_{D_1} is a dark Dirac fermion, that is unstable, and f_{D_2} is a second dark Dirac fermion, that is stable and escapes from detection. The production of f_{D_1} with a mass $m_{f_{D_1}}$ is possible via the exchange of a spin-1 Z_D with a mass of M_{Z_D} in the s-channel. In this model Z_D couples to quarks with a coupling constant g_q and couples to f_{D_1} with a coupling constant $g_{f_{D_1}}$. This model is based on a simplified DM model that had already been implemented in Feynrules website [6, 7]. The coupling between the dark vector boson Z_D and SM or dark fermion fields is considered to be either vector or axial-vector, which leads to the two interaction Lagrangians, given by

$$\mathscr{L}_{vector} = g_{q_V} \sum_q Z_{D_\mu}\bar{q}\gamma^\mu q + g_{f_{D_1}} Z_{D_\mu}\overline{f_{D_1}}\gamma^\mu f_{D_1} \tag{1}$$

and

$$\mathscr{L}_{axial-vector} = g_{q_A} \sum_q Z_{D_\mu}\bar{q}\gamma^\mu\gamma^5 q + g_{f_{D_1}} Z_{D_\mu}\overline{f_{D_1}}\gamma^\mu\gamma^5 f_{D_1}. \tag{2}$$

The interaction Lagrangian for $q\bar{q} \to Z_D$ is also considered to have both vector and axial-vector couplings such as the SM Z boson couplings. The corresponding two Lagrangians are

$$\mathcal{L}_{SM} = \bar{q}\gamma^{\mu}(g_q^V + g_q^A\gamma^5)qZ_{D_\mu} \tag{3}$$

and

$$\mathcal{L}_{DM} = \overline{f_{D_1}}\gamma^{\mu}(g_{f_{D_1}}^V + g_{f_{D_1}}^A\gamma^5)f_{D_1}Z_{D_\mu}. \tag{4}$$

Only decays required for the self-consistency of the model implemented, i.e. decays to quarks and unstable dark fermions, are taken into account in the definition of the mediator width. We do not consider any additional visible or invisible decays that may contribute to the decay width of the dark mediator, e.g. decays to SM leptons. This leads to a minimal decay width Γ_{min} of Z_D determined by the choices of g_q and $g_{f_{D_1}}$ as given by [7,8].

$$\Gamma_{min}^V = \frac{g_{f_{D_1}}^2 M_{Z_D}}{12\pi}\Big(1 + \frac{2m_{f_{D_1}}^2}{M_{Z_D}^2}\Big)\beta_{f_{D_1}}\theta(M_{Z_D} - 2m_{f_{D_1}}) + \sum_q \frac{3g_q^2 M_{Z_D}}{12\pi}\Big(1 + \frac{2m_q^2}{M_{Z_D}^2}\Big)\beta_q\theta(M_{Z_D} - 2m_q) \tag{5}$$

and

$$\Gamma_{min}^A = \frac{g_{f_{D_1}}^2 M_{Z_D}}{12\pi}\beta_{f_{D_1}}^3\theta(M_{Z_D} - 2m_{f_{D_1}}) + \sum_q \frac{3g_q^2 M_{Z_D}}{12\pi}\beta_q^3\theta(M_{Z_D} - 2m_q). \tag{6}$$

Here, $\beta = \sqrt{1 - \frac{4m_f^2}{M_{Z_D}}}$ is the fermion velocity in the rest frame of Z_D and $\theta(x)$ is the Heaviside step function. The maximal lifetime τ_{max} of Z_D is expressed in this study by the maximal decay length $c\tau_{max}$, which is given by

$$c\tau_{max} = \frac{c\hbar}{\Gamma_{min}}. \tag{7}$$

3 Study of maximal lifetime of the dark vector boson

3.1 One-dimensional parameter scans

Below we address an analytical study of $c\tau_{max}$ given by Eq. (7) of vector versus axial-vector Z_D's through 1-dimensional scans over the four free parameters of Eqs. (5) and (6), which are mass of the dark vector boson M_{Z_D}, the DM-particle mass $m_{f_{D_1}}$, and coupling constants of the dark vector boson to quarks g_q and to the unstable dark fermion $g_{f_{D_1}}$.

3.1.1 Maximal lifetimes of vector and axial-vector mediators

We are interested in investigating how $c\tau_{max}^V$ of a vector Z_D and $c\tau_{max}^A$ of an axial-vector Z_D are impacted by various free parameters that build up a decay width of Z_D as given by Eq. (7).

Figure 2 shows how $c\tau_{max}$ and Γ_{min} of vector and axial-vector Z_D's vary in a scan over g_q (left panel) and $g_{f_{D_1}}$ (right panel). In this figure $c\tau_{max}$ for both vector and axial-vector Z_D's has a plateau over a range of very weak couplings until it starts to decrease rapidly with the increase of g_q and $g_{f_{D_1}}$. The plateau behaviour of $c\tau_{max}$ in both panels of this figure is caused by the domination of the term, quark or DM, that is kept fixed over the other varying term. This term becomes dominant over the fixed term for large values of coupling, and hence we see an increase of Γ_{min} and, in turn, a drop of $c\tau_{max}$. The two panels indicate that $c\tau_{max}^A$ (red) is slightly longer than $c\tau_{max}^V$ (black) over the same range of g_q and $g_{f_{D_1}}$. Since $c\tau_{max}$ of a particle is the mathematical reciprocal of its Γ_{min}, the two quantities show two mirror images of each other, and hence it is seen that Γ_{min}^A (green) has very slightly lower values than Γ_{min}^V (blue) over the same range of g_q and $g_{f_{D_1}}$.

3
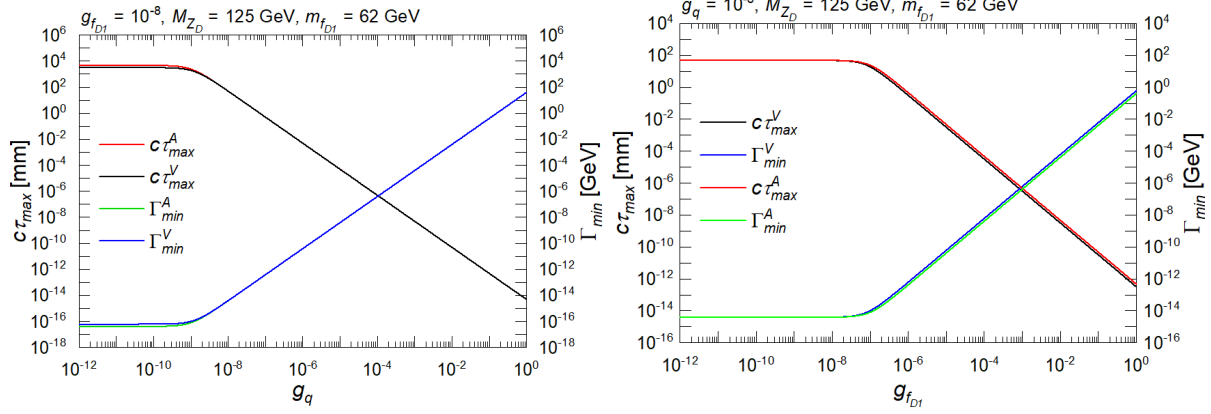
Figure 2: Variation of $c\tau_{max}$ (left axis) and Γ_{min} (right axis) of vector and axial-vector Z_D's for $M_{Z_D} = 125$ GeV and $m_{f_{D_1}} = 62$ GeV in a scan over g_q for $g_{f_{D_1}} = 10^{-8}$ (left) and over $g_{f_{D_1}}$ for $g_q = 10^{-8}$ (right).

Figure 3 shows how $c\tau_{max}$ and Γ_{min} of vector and axial-vector Z_D's vary in a scan over M_{Z_D} (left and middle panels) and $m_{f_{D_1}}$ (right panel). We find that the vector and axial-vector Z_D's show identical behavior over the same range of M_{Z_D}, which causes the two curves to fall on top of each other in the left panel of this figure, and consequently we only show the curve for the vector Z_D. The left panel also shows that $c\tau_{max}$ increases rapidly with the with the approach of M_{Z_D} to the kinematic threshold, indicated by the vertical dashed lines and defined by the on-shell regime of mediators where $M_{Z_D} > 2m_{f_{D_1}}$, while the middle panel shows that $c\tau_{max}$ increases more rapidly near the kinematic threshold of $m_{f_{D_1}} = 1.5$ GeV compared to a threshold of $m_{f_{D_1}} = 62$ GeV in case of the left panel. This indicates that $c\tau_{max}$ increases substantially for lower masses of Z_D. Similar to the behaviour in the two panels of Fig. 2, the right panel of Fig. 3 shows that $c\tau_{max}^A$ (red) is longer than $c\tau_{max}^V$ (black) over the same range of $m_{f_{D_1}}$ where the two curves intersect right at the threshold of $m_{f_{D_1}} = 0.5M_{Z_D}$, indicated by the vertical dashed line. The right panel of this figure shows also that $c\tau_{max}$ of both vector and axial-vector Z_D's has a plateau for values of $m_{f_{D_1}}$ away from the threshold. It is further found that $c\tau_{max}$ increases as $m_{f_{D_1}}$ approaches the threshold, while it boosts in the region very close to the threshold.
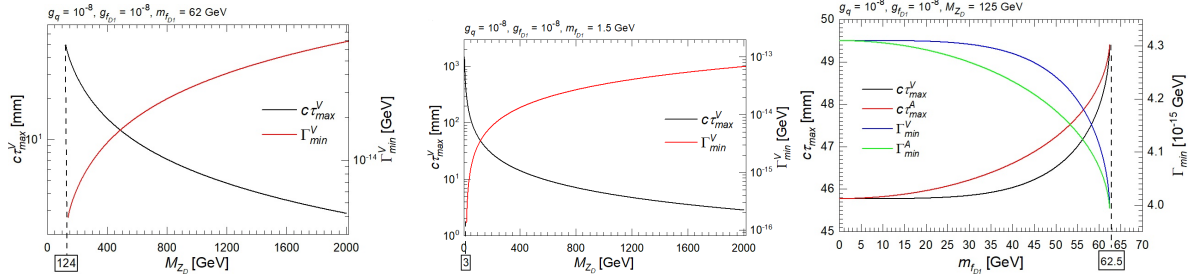
Figure 3: Variation of $c\tau_{max}^V$ (left axis) and Γ_{min}^V (right axis) of Z_D for $g_q = g_{f_{D_1}} = 10^{-8}$ in a scan over M_{Z_D} for $m_{f_{D_1}} = 62$ GeV (left) and $m_{f_{D_1}} = 1.5$ GeV (middle) as well as in a scan over $m_{f_{D_1}}$ for $M_{Z_D} = 125$ GeV (right).

3.1.2 How maximal lifetime of the dark vector boson varies in the scan over various free parameters

When a 1-dimensional parameter scan is performed, the impact of the other free parameters on the lifetime of a vector Z_D can also be studied, and accordingly, a full study of the influence of varying the values of free parameters on $c\tau_{max}^V$ is addressed below.

Figures 4−6 show the impact of varying $g_{f_{D_1}}$, M_{Z_D}, and $m_{f_{D_1}}$, respectively, on $c\tau_{max}^V$ in a scan over g_q. The three figures have the same black curve as that in the left panel of Fig. 2. In Fig. 4, the red curve shows a drop of $c\tau_{max}$ relative to the black curve by two orders of magnitude over the plateau region as $g_{f_{D_1}}$ is increased from 10^{-8} to 10^{-7}. In Fig. 5, the red curve shows a drop of $c\tau_{max}$ by about one order of magnitude over the plateau region and a drop by about half an order of magnitude over the range post

the plateau region relative to the black curve as M_{Z_D} is increased from 125 to 500 GeV. In Fig. 6, the red curve shows a drop of $c\tau_{max}$ by half an order of magnitude relative to the black curve over the plateau region, while the two curves superimpose over the range post the plateau region as $m_{f_{D_1}}$ is lowered from 62 to 31 GeV.
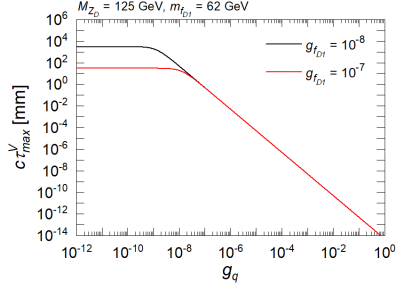
Figure 4: Impact of varying $g_{f_{D_1}}$ from 10^{-8} to 10^{-7} on $c\tau_{max}^V$ of Z_D in a scan over g_q for M_{Z_D} = 125 GeV and $m_{f_{D_1}}$ = 62 GeV.
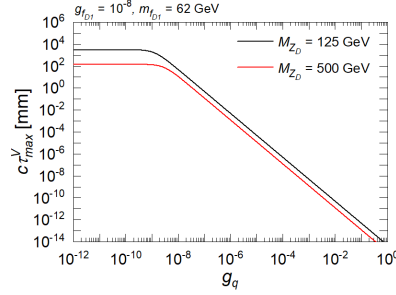
Figure 5: Impact of varying M_{Z_D} from 125 to 500 GeV on $c\tau_{max}^V$ of Z_D in a scan over g_q for $g_{f_{D_1}} = 10^{-8}$ and $m_{f_{D_1}} = 62$ GeV.
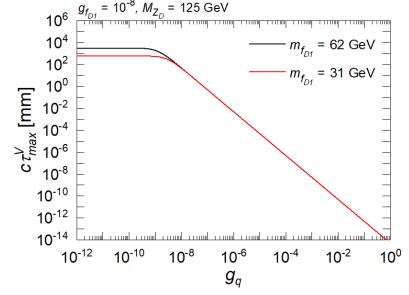
Figure 6: Impact of varying $m_{f_{D_1}}$ from 31 to 62 GeV on $c\tau_{max}^V$ of Z_D in a scan over g_q for $g_{f_{D_1}} = 10^{-8}$ and $M_{Z_D} = 125$ GeV.

Figures 7−9 show the impact of varying g_q, M_{Z_D}, and $m_{f_{D_1}}$, respectively, on $c\tau_{max}^V$ in a scan over $g_{f_{D_1}}$. The three figures have the same black curve as that in the right panel of Fig. 2. In Fig. 7, the red curve shows a drop of $c\tau_{max}$ relative to the black curve by two orders of magnitude over the plateau region as g_q is increased from 10^{-8} to 10^{-7}. In Fig. 8, as M_{Z_D} is increased from 125 to 500 GeV, the red curve shows a drop of $c\tau_{max}$ by half an order of magnitude relative to the black curve over the plateau region and a drop by about one order of magnitude over the range post the plateau region. In Fig. 9, as $m_{f_{D_1}}$ is lowered from 62 to 31 GeV, the red curve shows identical $c\tau_{max}$ to that for the black curve over the plateau region, while the red curve shows a drop of $c\tau_{max}$ relative to the black curve by about half an order of magnitude over the range beyond the plateau region.
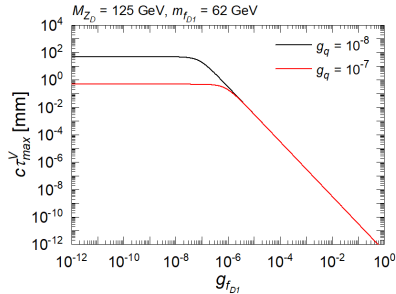
Figure 7: Impact of varying g_q from 10^{-8} to 10^{-7} on $c\tau_{max}^V$ of Z_D in a scan over $g_{f_{D_1}}$ for M_{Z_D} = 125 GeV and $m_{f_{D_1}}$ = 62 GeV.
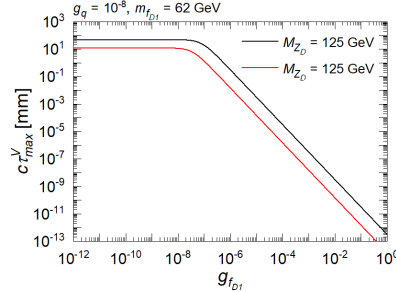
Figure 8: Impact of varying M_{Z_D} from 125 to 500 GeV on $c\tau_{max}^V$ of Z_D in a scan over $g_{f_{D_1}}$ for $g_q = 10^{-8}$ and $m_{f_{D_1}} = 62$ GeV.
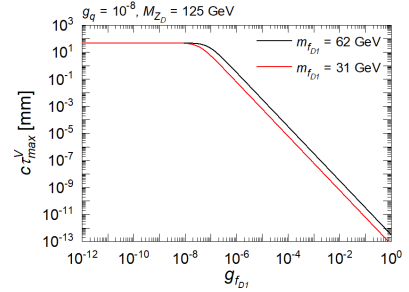
Figure 9: Impact of varying $m_{f_{D_1}}$ from 31 to 62 GeV on $c\tau_{max}^V$ of Z_D in a scan over $g_{f_{D_1}}$ for $g_q = 10^{-8}$ and $M_{Z_D} = 125$ GeV.

Figures 10−12 show the impact of varying g_q, $g_{f_{D_1}}$, and $m_{f_{D_1}}$, respectively, on $c\tau_{max}^V$ in a scan over M_{Z_D} with the kinematic threshold indicated by the vertical dashed line. The three figures have the same black curve as that in the left panel of Fig. 3. In Fig. 10, the red curve shows a drop of $c\tau_{max}$ relative to the black curve by two orders of magnitude as g_q is increased from 10^{-8} to 10^{-7}. In Fig. 11, as $g_{f_{D_1}}$ is increased from 10^{-8} to 10^{-7}, the red curve shows a drop of $c\tau_{max}$ relative to the black curve by one order of magnitude except at the threshold where the drop is slightly less than one order of magnitude. In Fig. 12, as $m_{f_{D_1}}$ is lowered from 62 to 31 GeV, the red curve shows identical $c\tau_{max}$ to that for the black curve except that the red curve extends to a threshold of 62 GeV versus a threshold of 124 GeV in the case of the black curve.

5
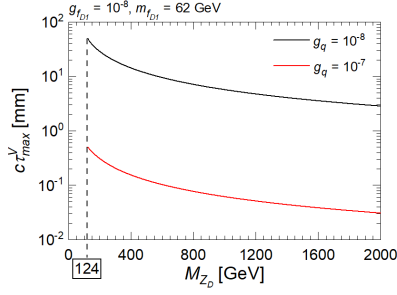
Figure 10: Impact of varying g_q from 10^{-8} to 10^{-7} on $c\tau_{max}^V$ of Z_D in a scan over M_{Z_D} for $g_{f_{D_1}} = 10^{-8}$ and $m_{f_{D_1}} = 62$ GeV.
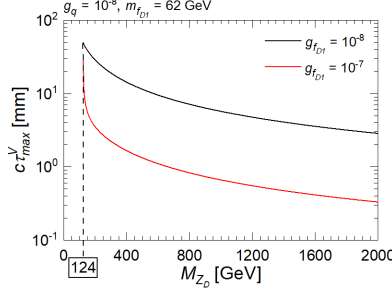
Figure 11: Impact of varying $g_{f_{D_1}}$ from 10^{-8} to 10^{-7} on $c\tau_{max}^V$ of Z_D in a scan over M_{Z_D} for $g_q = 10^{-8}$ and $m_{f_{D_1}} = 62$ GeV.
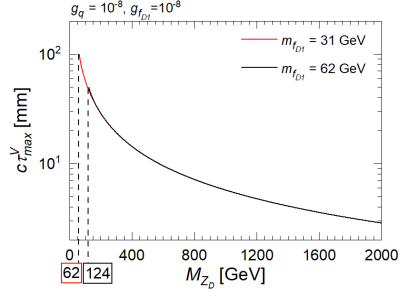
Figure 12: Impact of varying $m_{f_{D_1}}$ from 31 to 62 GeV on $c\tau_{max}^V$ of Z_D in a scan over M_{Z_D} for $g_q = 10^{-8}$ and $g_{f_{D_1}} = 10^{-8}$.

Figures 13−15 show the impact of varying g_q, $g_{f_{D_1}}$, and M_{Z_D}, respectively, on $c\tau_{max}^V$ in a scan over $m_{f_{D_1}}$ with the threshold indicated by the vertical dashed line. The three figures have the same black curve as that in the right panel of Fig. 3. In Fig. 13, as g_q is increased from 10^{-8} to 10^{-7}, the red curve shows an increase of $c\tau_{max}$ relative to the black curve by about 4 mm in the region far from the threshold with this increase tending to zero near the kinematic threshold. In Fig. 14, as $g_{f_{D_1}}$ is increased from 10^{-8} to 10^{-7}, the red curve shows a drop of $c\tau_{max}$ relative to the black curve by about 40 mm except for the region near threshold where the drop becomes less than 40 mm until it is about 25 mm right at the threshold. In Fig. 15, as M_{Z_D} is increased from 125 to 500 GeV, the red curve shows a drop of $c\tau_{max}$ relative to the black curve by about 35 mm and extends to a threshold of 250 GeV versus a threshold of 62.5 GeV for the black curve.
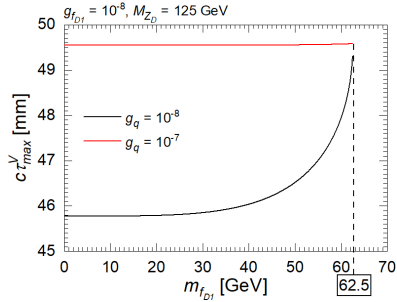
Figure 13: Impact of varying g_q from 10^{-8} to 10^{-7} on $c\tau_{max}^V$ of Z_D in a scan over $m_{f_{D_1}}$ for $g_{f_{D_1}} = 10^{-8}$ and $m_{f_{D_1}} = 62$ GeV.
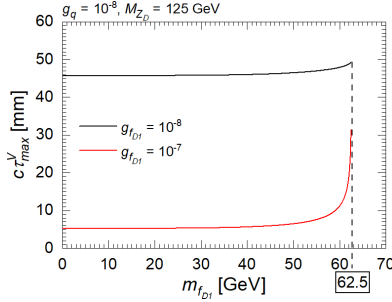
Figure 14: Impact of varying $g_{f_{D_1}}$ from 10^{-8} to 10^{-7} on $c\tau_{max}^V$ of Z_D in a scan over $m_{f_{D_1}}$ for $g_q = 10^{-8}$ and $m_{f_{D_1}} = 62$ GeV.
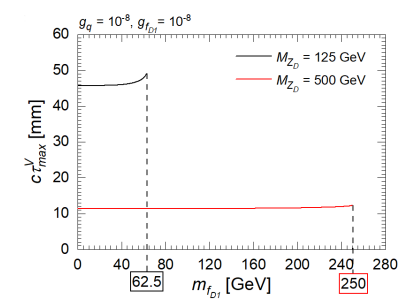
Figure 15: Impact of varying M_{Z_D} from 125 to 500 GeV on $c\tau_{max}^V$ of Z_D in a scan over $m_{f_{D_1}}$ for $g_q = 10^{-8}$ and $g_{f_{D_1}} = 10^{-8}$.

3.1.3 Contribution of quarks and DM to maximal lifetime of the dark vector boson

We investigate how much each of the quark and DM terms in Eq. (5) contributes to $c\tau_{max}^V$ of Z_D in Figs. 16−19. DM in Eq. (5) is meant to be the unstable dark fermions f_{D_1} or simply f_D, which has to be distinguished from the stable dark fermions f_{D_2} in the final state of the current decay mode. The upper panels of the four figures show the contribution of either the quark term, DM term, or both terms in Eq. (5) to $c\tau_{max}^V$ in a 1-dimensional parameter scan over g_q, $g_{f_{D_1}}$, M_{Z_D}, and $m_{f_{D_1}}$, respectively, while the lower panels of the figures show the ratio between the two contributions of quark and DM terms to $c\tau_{max}^V$ in the scan over the same free parameters.

The upper panel of Fig. 16 has the same black curve in the left panel of Fig. 2, which shows the contribution of both quark and DM terms in Eq. (5) to $c\tau_{max}^V$ in a scan over g_q. In this scan, the black curve in this panel shows a plateau behavior of $c\tau_{max}$ caused by the DM term being highly dominant over the quark term and unchanged because of being g_q-independent, while the plateau starts to vanish at equal contribution of both terms followed by the quark term being highly dominant over the DM term and causing $c\tau_{max}$ to decrease drastically as g_q increases. The red curve in this panel shows a monotonic decrease of $c\tau_{max}$ because of the consideration of the quark term only that is g_q-dependent. The upper panel of Fig. 17 has

the same black curve in the right panel of Fig. 2, which shows the contribution of both quark and DM terms of Eq. (5) to $c\tau_{max}^V$ in a scan over $g_{f_{D_1}}$. The black and red curves of this panel can be described similarly as the black and red curves of the upper panel of Fig. 16 except that the scan in this panel is over $g_{f_{D_1}}$ and that the red curve of this panel belongs to the consideration of the DM term only. The lower panels of Figs. 16 and 17 show that the ratio between the contributions of the two terms takes all the values below and above 1 over the entire ranges of scan over g_q and $g_{f_{D_1}}$.
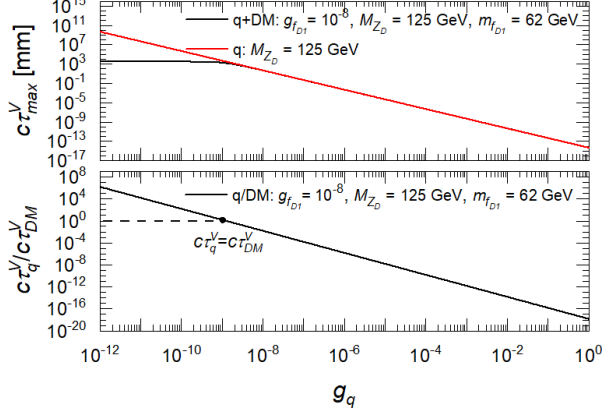
Figure 16: Variation of $c\tau_{max}^V$ of Z_D showing the contribution of quark term in Eq. (5) (top) and variation of the quark-to-DM contribution ratio (bottom), both against g_q for $g_{f_{D_1}} = 10^{-8}$, $M_{Z_D} = 125$ GeV, and $m_{f_{D_1}} = 62$ GeV.
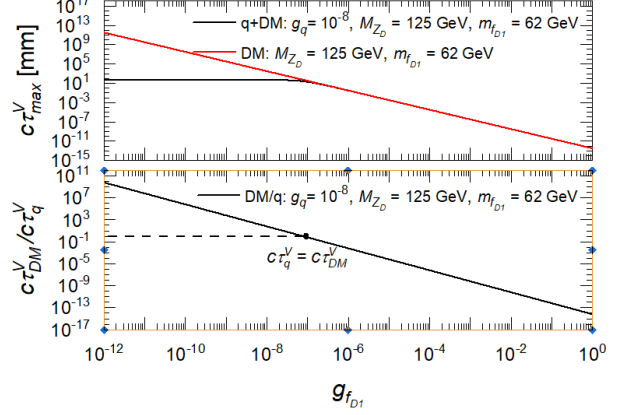
Figure 17: Variation of $c\tau_{max}^V$ of Z_D showing the contribution of DM term in Eq. (5) (top) and variation of the DM-to-quark contribution ratio (bottom), both against $g_{f_{D_1}}$ for $g_q = 10^{-8}$, $M_{Z_D} = 125$ GeV, and $m_{f_{D_1}} = 62$ GeV.
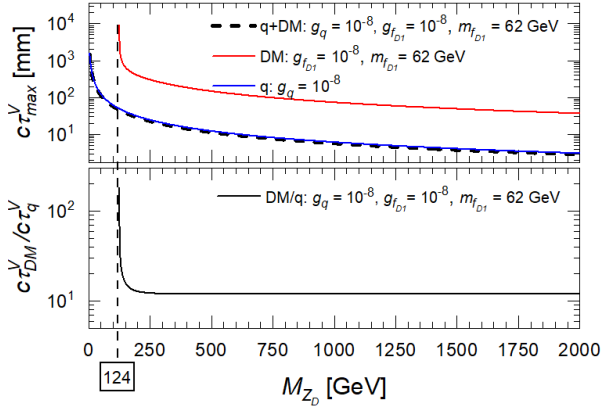
Figure 18: Variation of $c\tau_{max}^V$ of Z_D showing the contribution of each of quark and DM terms in Eq. (5) (top) and variation of the DM-to-quark contribution ratio (bottom), both against M_{Z_D} for $g_q = g_{f_{D_1}} = 10^{-8}$ and $m_{f_{D_1}} = 62$ GeV.
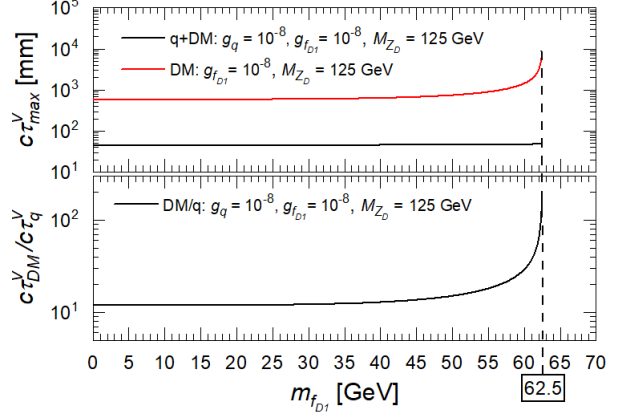
Figure 19: Variation of $c\tau_{max}^V$ of Z_D showing the contribution of DM term in Eq. (5) (top) and variation of the DM-to-quark contribution ratio (bottom), both against $m_{f_{D_1}}$ for $g_q = g_{f_{D_1}} = 10^{-8}$ and $M_{Z_D} = 125$ GeV.

The upper panel of Fig. 18 has the same black curve in the left panel of Fig. 3, which shows the contribution of both quark and DM terms in Eq. (5) to $c\tau_{max}^V$ in a scan over M_{Z_D} with the threshold indicated by a vertical dashed line. The red curve in this panel is obtained by considering the DM term only, which causes $c\tau_{max}$ to increase by one order of magnitude relative to the black curve, while the blue curve is obtained by considering the quark term only, which causes $c\tau_{max}$ to increase slightly relative to the black curve. The blue curve extends to zero as it does not follow the on-shell regime of mediators due to the removal of the DM term. The upper panel of Fig. 19 has the same black curve in the right panel of Fig. 3, which shows the contribution of both quark and DM terms to $c\tau_{max}^V$ in a scan over $m_{f_{D_1}}$ with the threshold indicated by a vertical dashed line. The red curve in this panel is obtained by considering the DM term only, which causes $c\tau_{max}$ to increase by one order of magnitude over the region far from threshold and by two orders of magnitude right at the threshold compared to the black curve. The lower

7

panels of Figs. 18 and 19 show that that the ratio between the contributions of the two terms has a lower limit of 10 for the given values of free parameters over ranges of scan of $125 - 2000$ GeV and $0.1 - 62.5$ GeV over M_{Z_D} and $m_{f_{D_1}}$, respectively.

3.2 Two-dimensional parameter scans

We investigate how $c\tau_{max}$ of vector and axial-vector Z_D's varies with various 2-dimensional parameter scans using colormaps. The scans are performed over the four free parameters of Eqs. (5) and (6), which are the same parameters used for the 1-dimensional parameter scans. Two 2-dimensional scans over the parameter pairs $(g_q, g_{f_{D_1}})$ and $(M_{Z_D}, m_{f_{D_1}})$ are addressed in the main text below of this study, while the rest of the scans are addressed in the appendices to provide a complete picture.
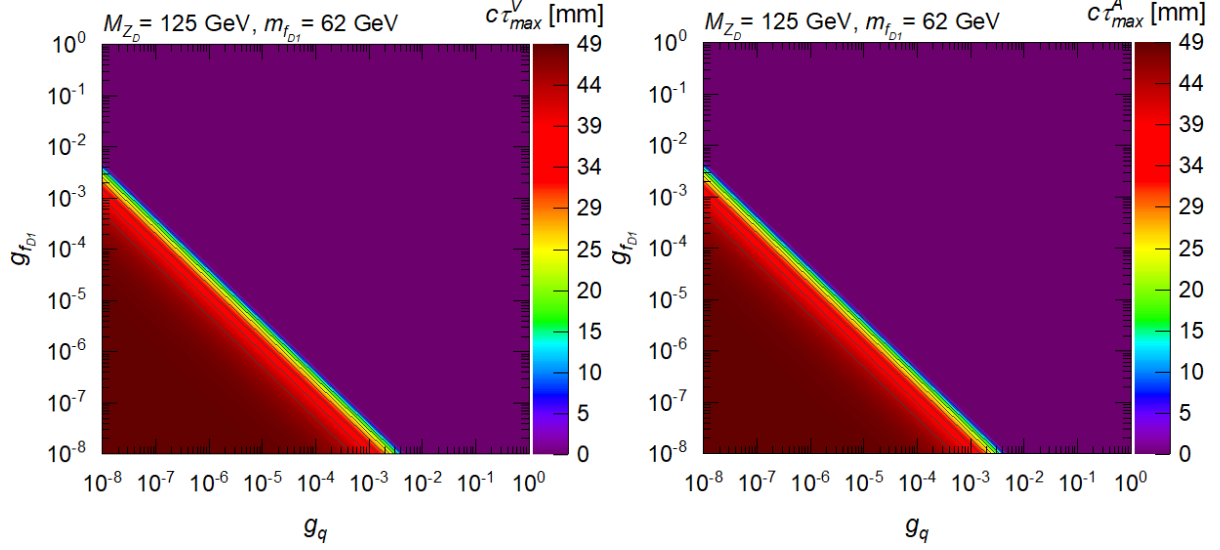
Figure 20: Variation of $c\tau_{max}^V$ (left panel) and $c\tau_{max}^A$ (right panel) of Z_D for $M_{Z_D} = 125$ GeV and $m_{f_{D_1}} = 62$ in a scan over the g_q-$g_{f_{D_1}}$ plane.
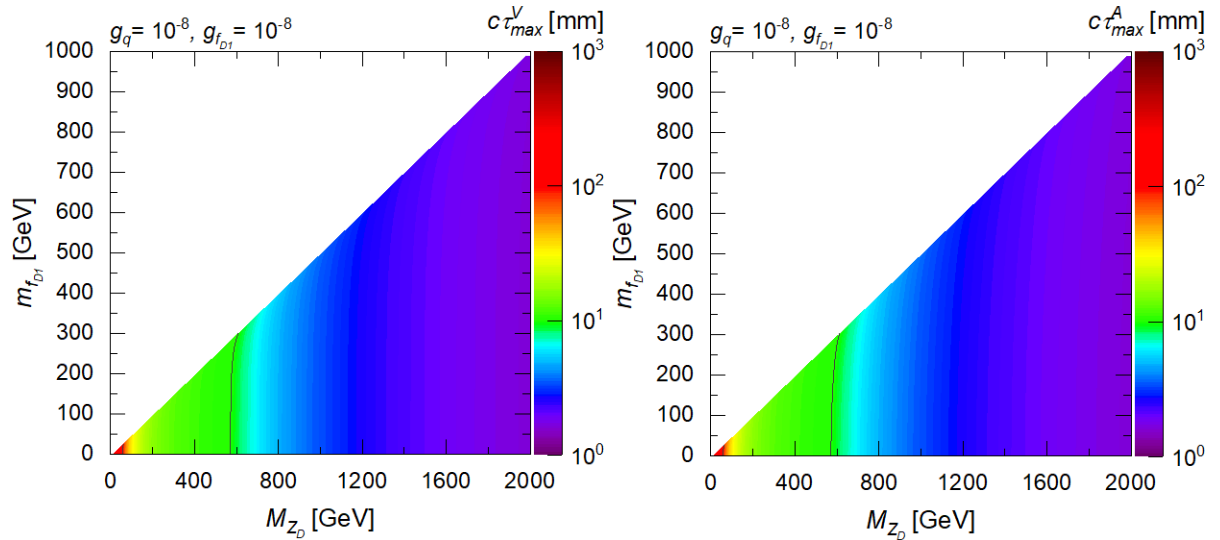
Figure 21: Variation of $c\tau_{max}^V$ (left panel) and $c\tau_{max}^A$ (right panel) of Z_D in a scan over the M_{Z_D}-$m_{f_{D_1}}$ plane for $g_q = g_{f_{D_1}} = 10^{-8}$.

Figure 20 shows how $c\tau_{max}^V$ (left panel) and $c\tau_{max}^A$ (right panel) of Z_D varies in a scan over the g_q-$g_{f_{D_1}}$ plane for $M_{Z_D} = 125$ GeV. The two panels of this figure are very slightly different and show that a longer $c\tau_{max}^V$ of Z_D is associated with lower values of g_q and $g_{f_{D_1}}$ where the dark purple region corresponds to prompt Z_D's with $c\tau_{max}^V < 1$ mm, while the rest of colors correspond to LL Z_D's with $c\tau_{max}^V$ in the range

8

of $1 - 49$ mm.

Figure 21 shows how $c\tau^V_{max}$ and $c\tau^A_{max}$ of Z_D vary in a scan over the M_{Z_D}-$m_{f_{D_1}}$ plane. The two panels of this figure indicate how a longer $c\tau_{max}$ of both vector and axial-vector Z_D's is associated with lower values of M_{Z_D} and, in turn, with lower values of $m_{f_{D_1}}$ as a requirement for on-shell Z_D's. Both vector and axial-vector Z_D's have almost the same behavior of $c\tau_{max}$ in this scan.

4 Study of the cross section of a dark vector boson

4.1 Maximal scaled generator-level cross section of vector and axial-vector mediators

The on-shell Z_D is the most promising regime as it is more likely to be measured at the LHC than the off-shell Z_D. The production cross section of the on-shell Z_D is enhanced near $q^2 \sim M^2_{Z_D}$ where q (GeV) is the momentum transfer as calculated from the two partons contributing to the hard process after the initial state radiation, which is equivalent to the momentum of the DM pair. The maximal scaled generator cross section σ^{scl}_{max}, given in arbitrary unit (a.u.), of an on-shell Z_D can be given by [7]

$$\sigma^{scl}_{max} \propto \frac{g_q^2 g_{f_{D_1}}^2}{\Gamma_{min}}. \tag{8}$$

4.1.1 One-dimensional parameter scans

The upper panels of Fig. 22 show how $\sigma^{scl,V}_{max}$ and $\sigma^{scl,A}_{max}$ (upper left) and $\sigma^{scl,V}_{max}$ (upper right) of Z_D vary in a scan over g_q and $g_{f_{D_1}}$, respectively, while the lower panels of this figure show the ratio between the two contributions of quark and DM terms to $\sigma^{scl,V}_{max}$ where this ratio takes values below and above 1 as indicated on each plot. The The upper left panel shows how a larger σ^{scl}_{max} is associated with a stronger g_q for both vector and axial-vector Z_D's until a saturation of σ^{scl}_{max} is reached at which the DM and quark terms in Eq. (8) have an equal contribution to σ^{scl}_{max}. An axial-vector Z_D has a very slightly larger σ^{scl}_{max} compared to a vector Z_D over the range of g_q before the plateau is reached. The curves for vector and axial-vector Z_D's fall on top of each other because of their identical behavior, and we only show the behavior of vector Z_D in the upper right panel. The plateau behavior in the upper right panel is more visible over the range of $g_{f_{D_1}} > 1$, which is not shown in this figure.
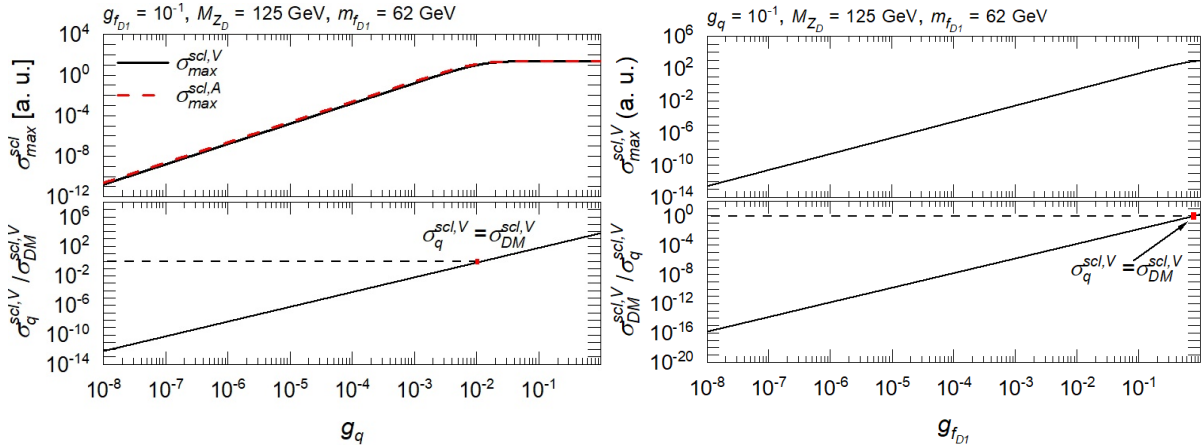
Figure 22: Variation of σ^{scl}_{max}, given by Eq. (8), for $m_{f_{D_1}} = 62$ GeV and $M_{Z_D} = 125$ GeV in a scan over g_q for $g_{f_{D_1}} = 10^{-1}$ (left) of vector (black) and axial-vector (red) Z_D's and in a scan over $g_{f_{D_1}}$ for $g_q = 10^{-1}$ (right) of vector Z_D's.

4.1.2 Two-dimensional parameter scans

Two scans over the planes of g_q-$g_{f_{D_1}}$ and M_{Z_D}-$m_{f_{D_1}}$ are addressed in this section, while two additional scans over the planes of g_q-M_{Z_D} and $g_{f_{D_1}}$-$m_{f_{D_1}}$ are addressed in the appendices for completeness.
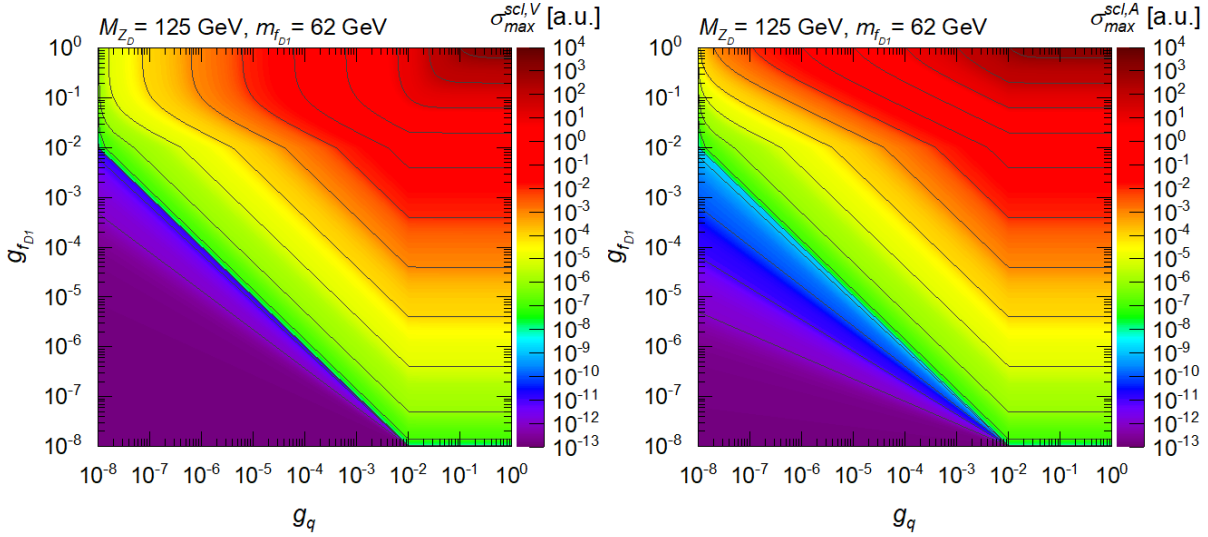
Figure 23: Variation of $\sigma_{max}^{scl,V}$ (left panel) and $\sigma_{max}^{scl,A}$ (right panel) in a scan over the g_q-$g_{f_{D_1}}$ plane for $M_{Z_D} = 125$ GeV and $m_{f_{D_1}} = 62$ GeV.

Figure 23 shows how $\sigma_{max}^{scl,V}$ (left panel) and $\sigma_{max}^{scl,A}$ (right panel), scaled from Eq. (8), vary in a scan over the g_q-$g_{f_{D_1}}$ plane. The two panels of this figure show that for both vector and axial-vector a larger σ_{max}^{scl} (a.u.) is associated with higher g_q and $g_{f_{D_1}}$ and vice versa. However, the figure also shows that the behavior of $\sigma_{max}^{scl,V}$ is slightly different from $\sigma_{max}^{scl,A}$.
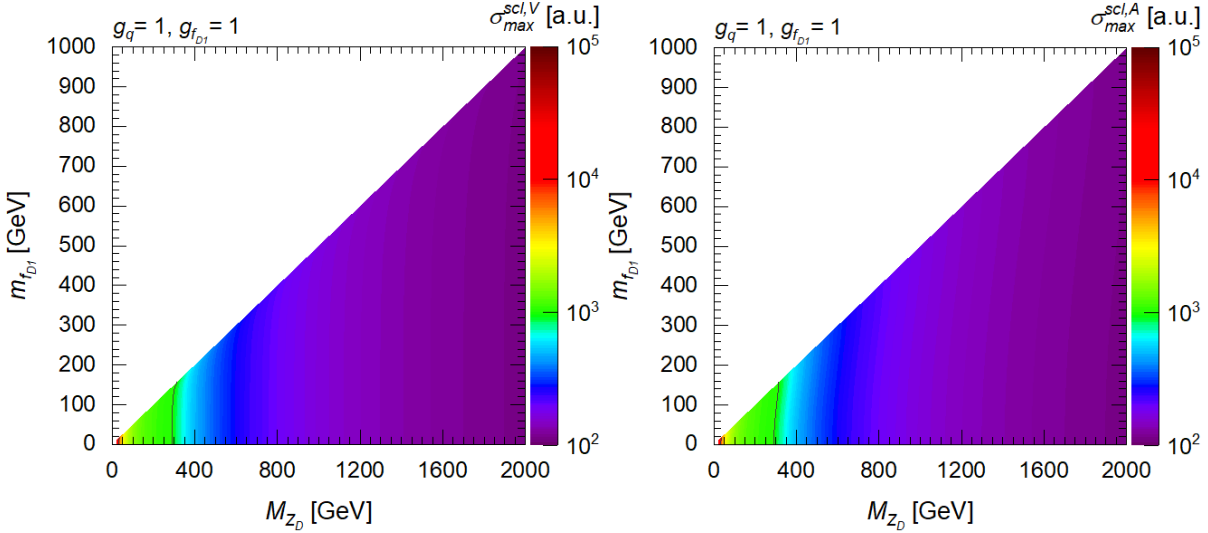
Figure 24: Variation of $\sigma_{max}^{scl,V}$ (left panel) and $\sigma_{max}^{scl,A}$ (right panel) in a scan over the M_{Z_D}-$m_{f_{D_1}}$ plane for $g_q = 1$ and $g_{f_{D_1}=1}$.

Figure 24 shows how $\sigma_{max}^{scl,V}$ (left panel) and $\sigma_{max}^{scl,A}$ (right panel), scaled from Eq. (8), vary in a scan over the g_q-$g_{f_{D_1}}$ plane. The two panels of this figure show that for both vector and axial-vector Z_D's a larger σ_{max}^{scl} (a.u.) is associated with lighter Z_D's and lighter f_{D_1}'s and vice versa. However, the figure also shows that the behavior of $\sigma_{max}^{scl,V}$ is very slightly different from $\sigma_{max}^{scl,A}$.

4.2 Absolute production cross section and analytical maximal lifetime of the dark vector boson

The top and bottom quarks are excluded from calculation of the production cross section $\sigma(pp \rightarrow Z_D)$, which causes that 2.54 GeV is the lowest M_{Z_D} that can be reached in our MC simulation based on the charm-quark mass of 1.27 GeV as the heaviest quark of the four quarks considered as indicated in Fig. 25.
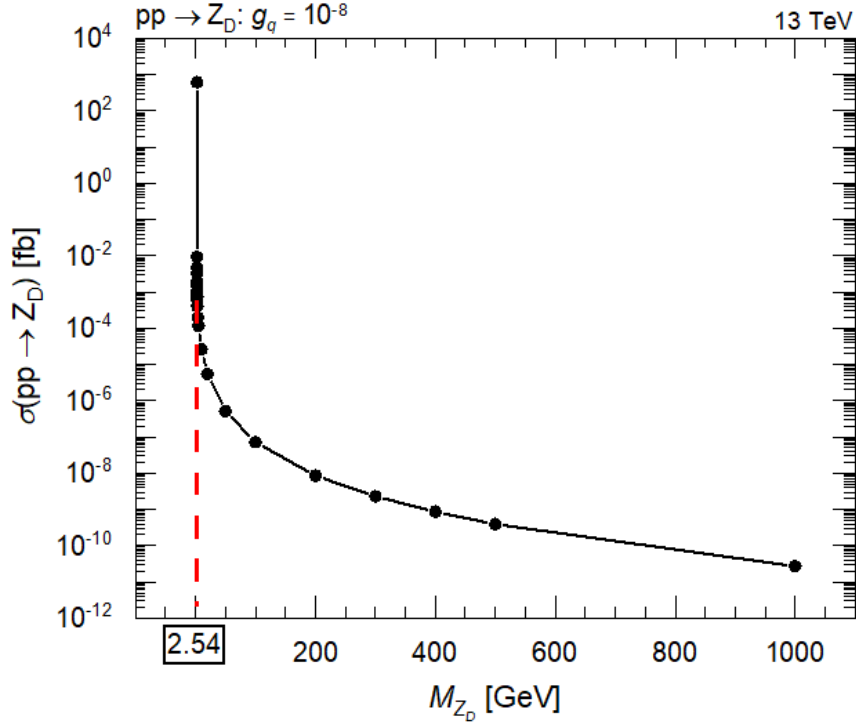
Figure 25: MC simulation of the variation of production cross section $\sigma(pp \to Z_D)$ against M_{Z_D} for Run 2 of the LHC and $g_q = 10^{-8}$.
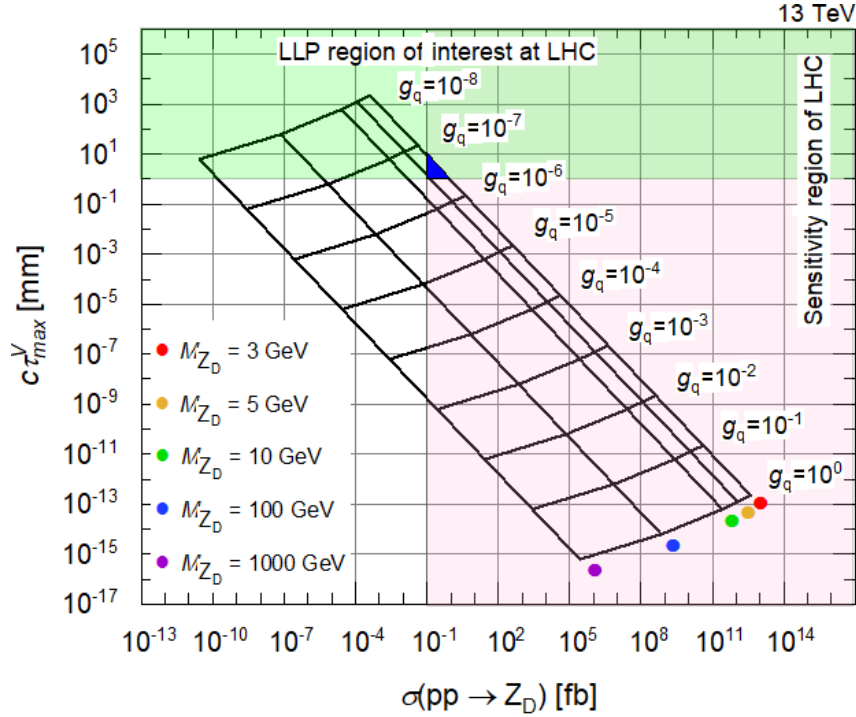
Figure 26: Two overlapped 1-dimensional plots showing how the MC simulated production cross section $\sigma(pp \to Z_D)$ and the analytically calculated $c\tau_{max}^V$ of Z_D vary against each other for various values of g_q and M_{Z_D} and Run 2 of the LHC.

Figure 26 shows how the simulated production cross section $\sigma(pp \to Z_D)$, under the implementation of the direct-coupling model addressed in Ref. [5] through MADGRAPH5_aMC@NLO v2.7.0, varies with

the corresponding analytically-calculated $c\tau_{max}^V$ of Z_D making use of Eqs. (5) and (7). The figure is an incorporation of two 1-dimensional plots where one of them is produced for various values of g_q over the ranges of $10^{-8} - 1$, while the other is produced for various values of M_{Z_D} over the range of $3-1000$ GeV. On a logarithmic scale of $\sigma(pp \to Z_D)$ and $c\tau_{max}^V$, they are found to be directly and inversely proportional to each other for the same M_{Z_D} and g_q, respectively. The LLP region of interest at the LHC is shaded in green, while the region where the LHC can be sensitive to the measurement of Z_D is shaded in pink. The *sensitive region* here is broadly defined as the region where at least ten Z_D events would get *produced* for 130 fb^{-1} worth of recorded luminosity at the LHC, equivalent to the amount of data taken by ATLAS and CMS in Run 2. Acceptances and efficiencies are not taken into account in the estimate of $\sigma(pp \to Z_D)$. The small intersection region (blue triangle) of the two shades is the region where an LLP might have already been produced at the LHC. Long-lived Z_D's with masses above 5 GeV would not have been produced in appreciable quantities during Run 2 of the LHC. We have performed another investigation that is not addressed in this study with the consideration of the decay of a vector Z_D into two dark scalar bosons in the final state of two dimuons [9].

5   Lorentz boost of lifetime for a light dark vector boson

A dark vector boson Z_D produced with substantial momentum experiences a Lorentz boost of its lifetime, and in turn decay length, as observed in the laboratory frame, and in particular if it is light and has a large gamma factor. The components orthogonal to the direction of motion don't change, while the components parallel to the direction of motion change and can be boosted. In this context, we use a MC simulation for Run 2 of the LHC using the framework of MADGRAPH5_aMC@NLO v2.7.0 at leading order and using the model addressed in Ref. [5] to show how much the decay length $L_\perp$ of LL Z_D can be boosted in Lorentz transformation to the boosted component $L_\parallel$ in the scan over M_{Z_D}.

Figure 27 shows Lorentz boost of $c\tau_{Z_D}$ from $L_\perp$ (red) to $L_\parallel$ (blue) for two masses of Z_D, 1000 GeV (left) and 3 GeV (right). It is found that Lorentz boost factor for $M_{Z_D} = 3$ GeV is 400 times larger than that for $M_{Z_D} = 1000$ GeV. This is in support of the fact that a light LL Z_D is boosted in Lorentz transformation compared to heavier LL Z_D. The mass points, 3, 5, 10, 50, 100, 500, and 1000 GeV, of Z_D are chosen for which Lorentz boost factors are calculated and shown in Fig. 28. This figure shows how lifetime of a light Z_D is highly boosted compared to a heavier Z_D.
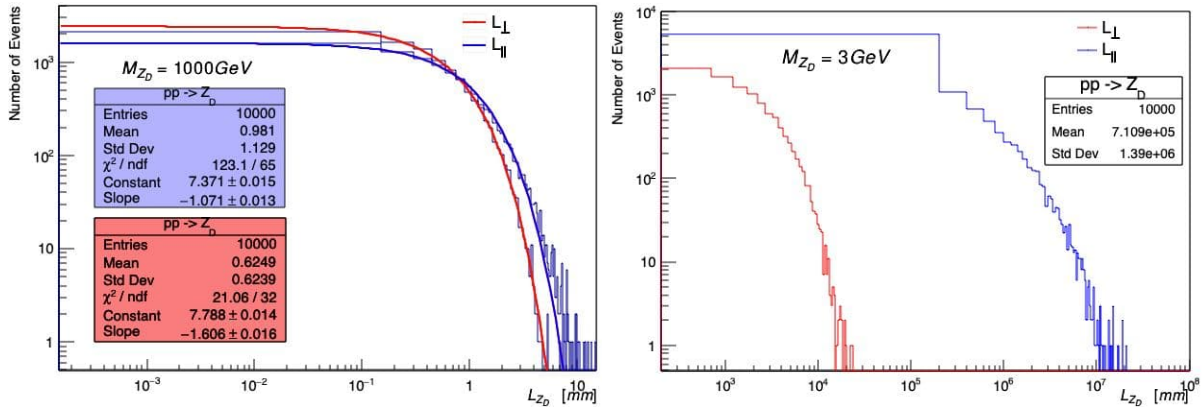
Figure 27: Number of events corresponding to the invariant decay length $L_\perp$ (red) and Lorentz transformed boosted component $L_\parallel$ (blue) of a vector Z_D for two masses of Z_D, 1000 GeV (left) and 3 GeV (right), both for $g_q = 10^{-8}$ and Run 2 of the LHC.
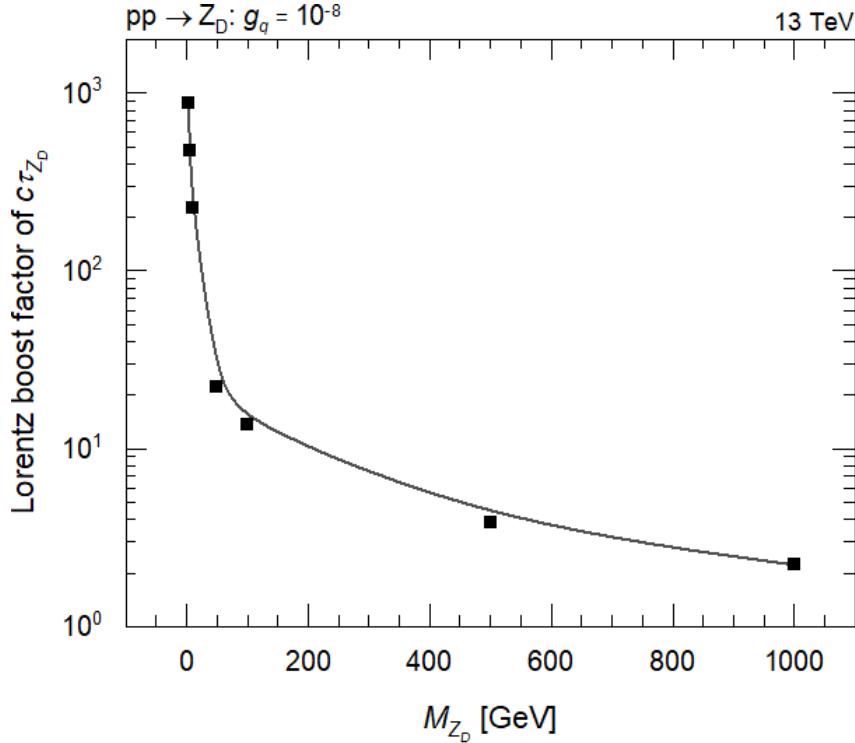
Figure 28: MC simulation showing how Lorentz boost factor of $c\tau_{Z_D}$ is expected to vary against M_{Z_D} for $g_q = 10^{-8}$ during Run 2 of the LHC.

6   Summary and conclusion

In the 1- and 2-dimensional parameter scans, a longer $c\tau_{max}$ of vector and axial-vector Z_D is associated with lower values of g_q, $g_{f_{D_1}}$, and M_{Z_D} and higher values of $m_{f_{D_1}}$. An axial-vector Z_D shows either a slightly higher or identical, but not lower, $c\tau_{max}$ compared to a vector Z_D. While $c\tau_{max}$ for on-shell vector and axial-vector Z_D's boosts upon the approach to the kinematic threshold of $m_{f_{D_1}} = 0.5M_{Z_D}$, it is found that $c\tau^A_{max}$ takes higher values than $c\tau^V_{max}$ over the entire scan range of $m_{f_{D_1}}$ and equal values to $c\tau^V_{max}$ right at the threshold and for very light f_{D_1}'s. In the 1-dimensional parameter scans over g_q and $g_{f_{D_1}}$, the two parameters are found to have upper limits below which $c\tau_{max}$ of a vector Z_D is unchanged where at such limits quarks and DM have equal contributions to $c\tau_{max}$. The DM contribution is found to have a higher contribution to $c\tau_{max}$ of Z_D than that of quarks by about two orders of magnitude at the threshold and by about one order of magnitude elsewhere for the given values of free parameters. The maximal scaled generator cross section σ^{scl}_{max} of vector and axial-vector Z_D's boosts with the increase of the coupling strengths of Z_D to quarks and the unstable dark fermions, g_q and $g_{f_{D_1}}$. In addition, it is found that σ^{scl}_{max} increases by the same number of orders of magnitude that M_{Z_D} decreases by. However, it is seen that σ^{scl}_{max} is highly influenced by changing the coupling constants g_q and $g_{f_{D_1}}$ compared to the impact of changing M_{Z_D}. In the 1-dimensional parameter scans over g_q and $g_{f_{D_1}}$, they are seen to have critical values above which σ^{scl}_{max} is unchanged. Our simulation calculations for $\sigma(pp \to Z_D)$ of a vector Z_D show that for low M_{Z_D} there could be a sufficient cross section for producing Z_D as an LLP. However, this region suffers from low kinematic acceptance of SM decay products. Although in principle there is a window for having produced an LLP in the mass range of $M_{Z_D} < 5$ GeV in Run 2 of the LHC, the lack of kinematic acceptance for the rather low-p_T SM fermions in the resulting final state prevents the experiments from detecting such an LLP. Consequently, an LL dark vector boson Z_D, with direct coupling to quarks, is not likely to be detected in Run 2 of the LHC due to this lack of sensitivity. We suggest to investigate dedicated triggers that are adapted to the particular kinematics and topology of such low-mass LL Z_D decays for Run 3. The lifetime of a light dark vector boson is found to be highly boosted for Run 2 of the LHC in Lorentz transformation compared to a heavier dark vector boson. This expectation is based on our MC simulation, which shows that the lifetime of vector Z_D is boosted by about three orders of magnitude if M_{Z_D} is dropped from 1000 to 3 GeV.

References

[1] Vera C. Rubin. A brief history of dark matter. In *The Dark Universe: Matter, Energy and Gravity*, pages 1–13. Cambridge University Press, Cambridge, 2004.

[2] Virginia Trimble. Existence and nature of dark matter in the universe. *Annu. Rev. Astron. Astr.*, 25(1):425–472, 1987.

[3] Bob Holdom. Two $U(1)$'s and epsilon charge shifts. *Phys. Lett. B*, 166(2):196–198, 1986.

[4] Lawrence Lee, Christian Ohm, Abner Soffer, and Tien-Tien Yu. Collider searches for long-lived particles beyond the standard model. *Prog. Part. Nucl. Phys.*, 106:210–255, 2019.

[5] J. A. Aguilar–Saavedra, J. A. Casas, J. Quilis, , and R. Ruiz de Austri. Multilepton dark matter signals. *J. High Energ. Phys.*, 2020, 69 (2020).

[6] Olivier Mattelaer and Eleni Vryonidou. Dark-matter production through loop-induced processes at the LHC: the s-channel mediator case. *Eur. Phys. J. C*, 75(9):436, 2015.

[7] Daniel Abercrombie *et al*. Dark matter benchmark models for early LHC Run-2 Searches: Report of the ATLAS/CMS dark matter forum. *Phys. Dark Universe*, 27:100371, 2020.

[8] Philip Harris, Valentin V. Khoze, Michael Spannowsky, and Ciaran Williams. Constraining dark sectors at colliders: Beyond the effective theory approach. *Phys. Rev. D*, 91(5):055009, 2015.

[9] Sven Dildick, Paul Padley, Wei Shi, Teruki Kamon, Hyunyong Kim, Alexei Safonov, Tamer Elkafrawy, Marcus Hohlmann, Mehdi Rahmani, and Alfredo Castaneda. Search for new bosons decaying into pairs of muons using Run 2 cms data. *CMS Analysis Note, CERN, with referee*, xx:xxxxxx, xxxx.

[10] Chiara Arina and Maria Eugenia Cabrera. Multi-lepton signatures at LHC from sneutrino dark matter. *J. High Energ. Phys.*, 2014, 100 (2014).

Appendices

7 Two-dimensional parameter scans for maximal lifetime of vector and axial-vector mediators

Below is the rest of the 2-dimensional parameter scans started in Sec. 3.2 towards an investigation of how $c\tau_{max}$ of vector and axial-vector Z_D's varies where a colormap is produced for each scan.
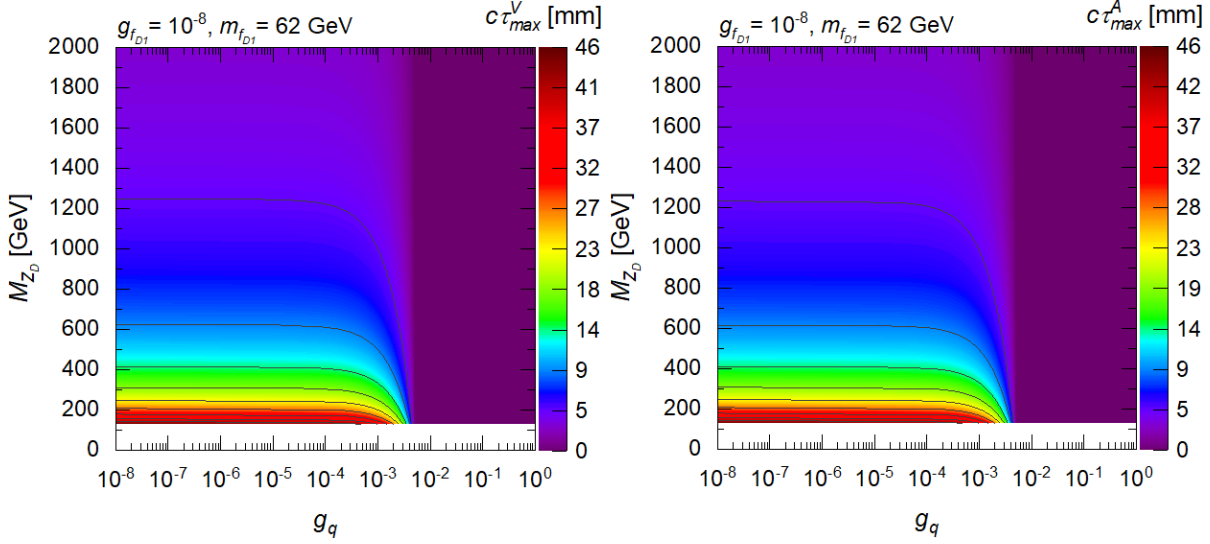
Figure 29: Variation of $c\tau_{max}$ in a scan over the g_q-M_{Z_D} plane. This plot is produced for $g_{f_{D_1}} = 10^{-8}$ and $m_{f_{D_1}} = 62$ GeV for a vector Z_D (left) and an axial-vector Z_D (right).

Figure 29 shows how $c\tau_{max}^V$ and $c\tau_{max}^A$ of Z_D vary in a scan over the g_q-M_{Z_D} plane. The two panels of this figure demonstrate that a longer $c\tau_{max}$ of both vector and axial-vector Z_D's is associated with lower g_q and M_{Z_D}. In addition, they show a similar behavior of $c\tau_{max}$ with a tiny difference between the two. However, changing g_q up to 10^{-4} has no impact on $c\tau_{max}$ for both vector and axial-vector Z_D's. At values higher than the upper limit of g_q mentioned above, it is found that $c\tau_{max}$ varies with the variation of both g_q and $g_{f_{D_1}}$.
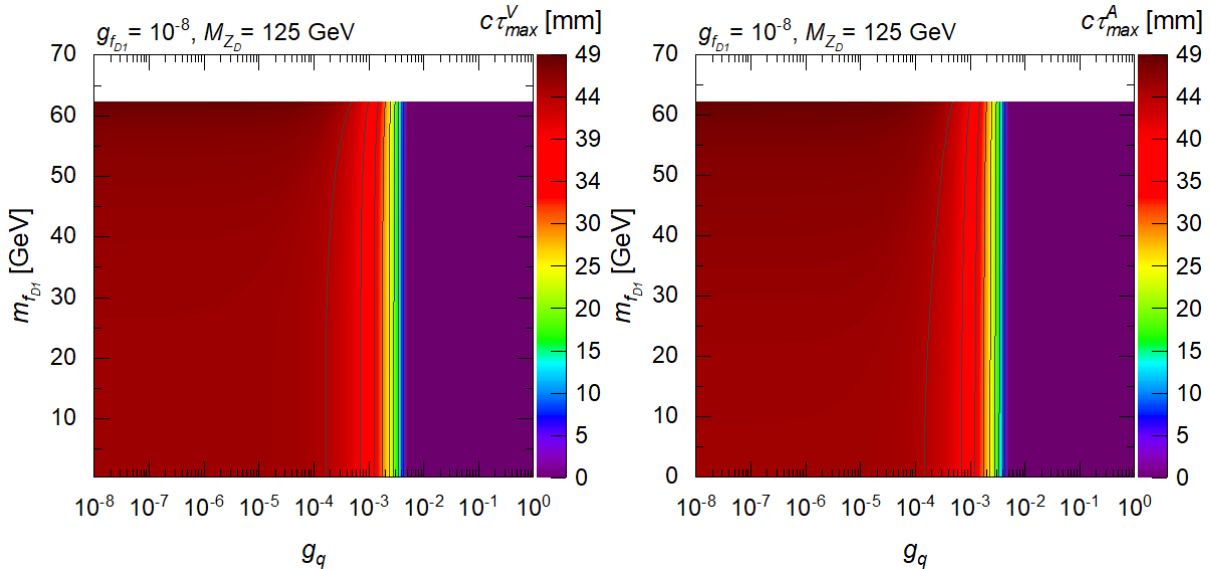
Figure 30: Variation of $c\tau_{max}$ in a scan over the g_q-$m_{f_{D_1}}$ plane. This plot is produced for $g_{f_{D_1}} = 10^{-8}$ and $M_{Z_D} = 125$ GeV for a vector Z_D (left) and an axial-vector Z_D (right).

Figure 30 shows how $c\tau_{max}^{V}$ and $c\tau_{max}^{A}$ of Z_D vary in a scan over the g_q-$m_{f_{D_1}}$ plane. The two panels of this figure show that a longer $c\tau_{max}$ of both vector and axial-vector Z_D's is associated with lower g_q, while varying $m_{f_{D_1}}$ has no impact on $c\tau_{max}$. Both vector and axial-vector Z_D's are seen to have almost the same behavior in this parameter scan.
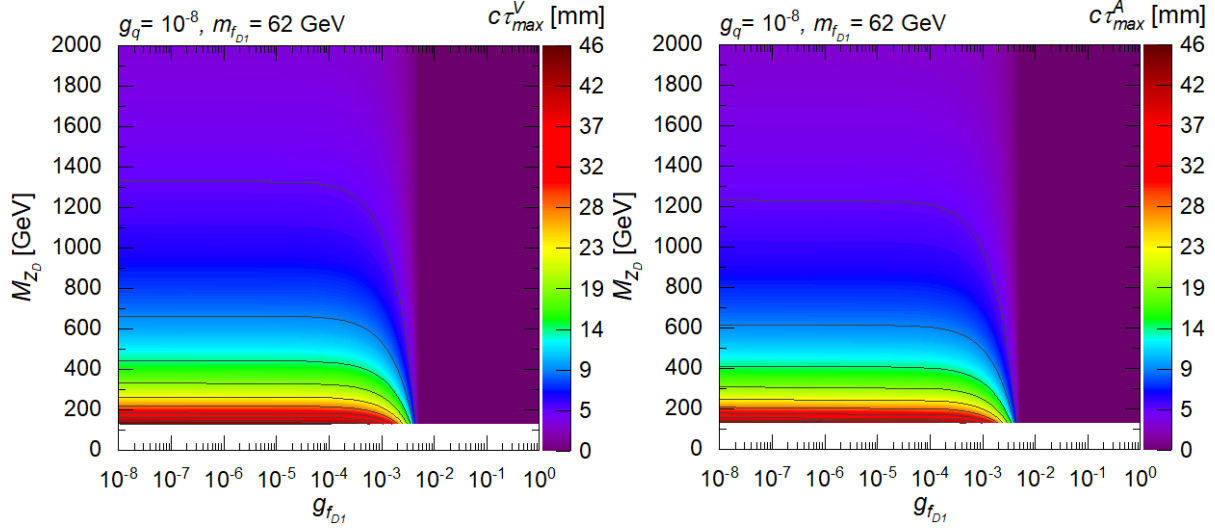
Figure 31: Variation of $c\tau_{max}$ in a scan over the $g_{f_{D_1}}$-M_{Z_D} plane. This plot is produced for $g_q = 10^{-8}$ and $m_{f_{D_1}} = 62$ GeV for a vector Z_D (left) and an axial-vector Z_D (right).

Figure 31 shows how $c\tau_{max}^{V}$ and $c\tau_{max}^{A}$ of Z_D vary in a scan over the $g_{f_{D_1}}$-M_{Z_D} plane. The two panels of this figure show a longer $c\tau_{max}$ of both vector and axial-vector Z_D's is associated with lower $g_{f_{D_1}}$ and M_{Z_D}. However, there is almost no difference between the behaviors of vector and axial-vector Z_D's in a scan over the $g_{f_{D_1}}$-M_{Z_D} plane.
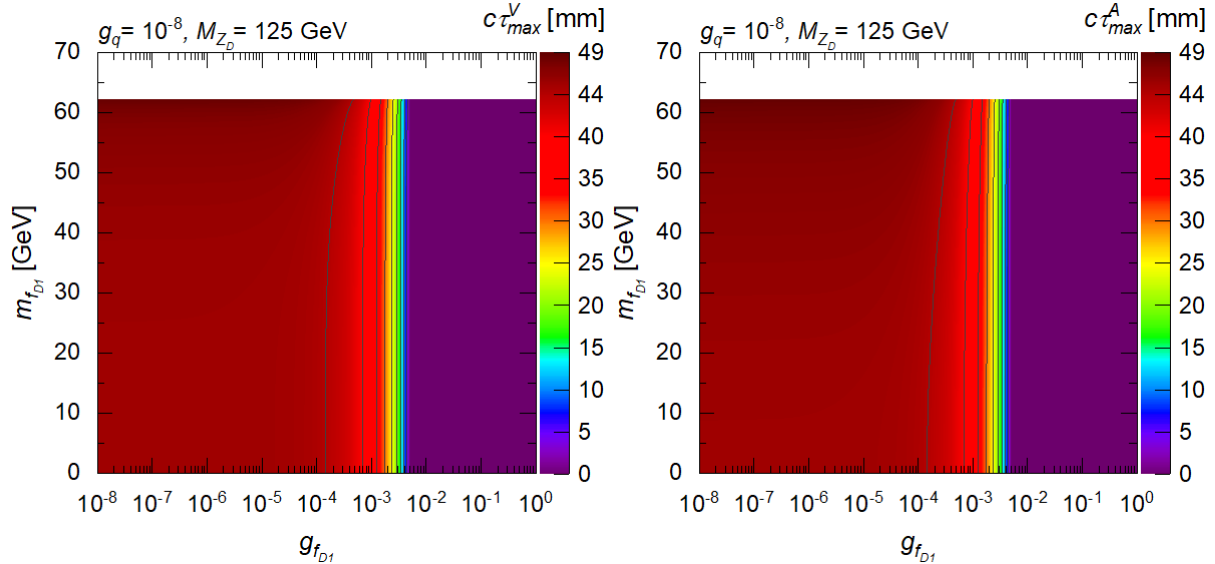
Figure 32: Variation of $c\tau_{max}$ in a scan over the $g_{f_{D_1}}$-$m_{f_{D_1}}$ plane. This plot is produced for $g_q = 10^{-8}$ and $M_{Z_D} = 125$ GeV for a vector Z_D (left) and an axial-vector Z_D (right).

Figure 32 shows how $c\tau_{max}^{V}$ and $c\tau_{max}^{A}$ of Z_D vary in a scan over the $g_{f_{D_1}}$-$m_{f_{D_1}}$ plane. The two panels of this figure show that a longer $c\tau_{max}$ of both vector and axial-vector Z_D's is associated with lower $g_{f_{D_1}}$, while varying $m_{f_{D_1}}$ has no impact on $c\tau_{max}$. Both vector and axial-vector Z_D's are seen to have almost the same behavior with the scan over $g_{f_{D_1}}$.

8 Two-dimensional parameter scans for scaled generator-level cross section of vector and axial-vector mediators

Below are two additional 2-dimensional parameter scans that completes the picture started in Sec. 4.1.2. Figure 33 shows how $\sigma_{max}^{scl,V}$ (left panel) and $\sigma_{max}^{scl,A}$ (right panel), scaled from Eq. (8), vary in a scan over the g_q-M_{Z_D} plane. The two panels of this figure show that for both vector and axial-vector Z_D's, σ_{max}^{scl} (a.u.) is mainly impacted by g_q, while the impact of M_{Z_D} is minor where the contour lines of σ_{max}^{scl} are seen to skew at higher M_{Z_D} towards higher values of g_q. However, the two panels of this figure show that a larger σ_{max}^{scl} is associated with higher g_q and vice versa. The figure also shows that the behavior of $\sigma_{max}^{scl,V}$ is very slightly different from $\sigma_{max}^{scl,A}$.
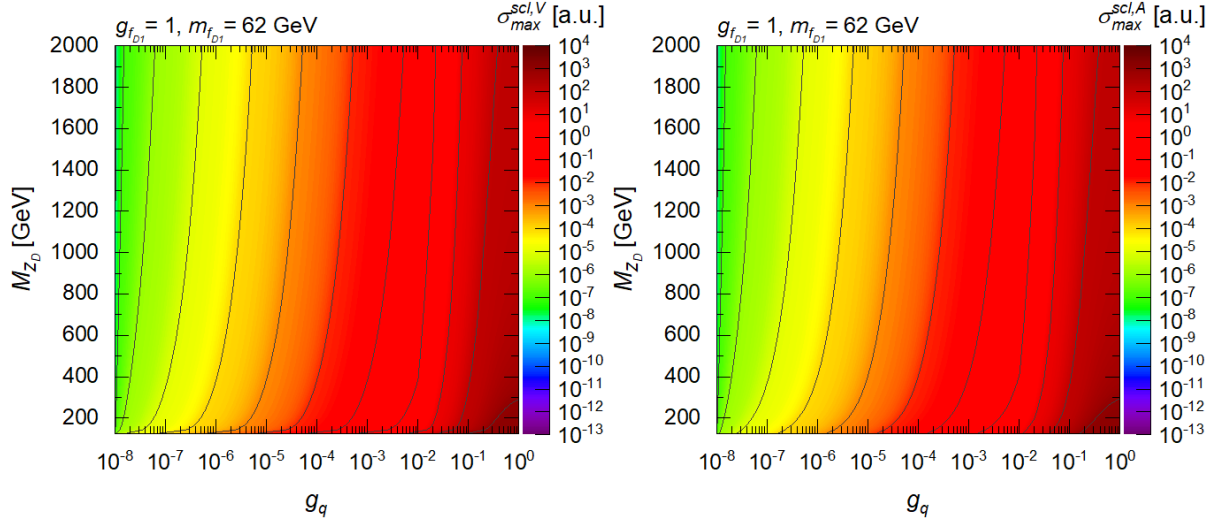
Figure 33: Variation of $\sigma_{max}^{scl,V}$ (left panel) and $\sigma_{max}^{scl,A}$ (right panel) in a scan over the g_q-M_{Z_D} plane for $g_{f_{D_1}} = 1$ and $m_{f_{D_1}} = 62$ GeV.

Figure 34 shows how $\sigma_{max}^{scl,V}$ (left panel) and $\sigma_{max}^{scl,A}$ (right panel), scaled from Eq. (8), vary in a scan over the $g_{f_{D_1}}$-$m_{f_{D_1}}$ plane. The two panels of this figure show that for both vector and axial-vector Z_D's, σ_{max}^{scl} (a.u.) is impacted only by $g_{f_{D_1}}$ with the absence of any impact of $m_{f_{D_1}}$. The two panels of this figure show that a larger σ_{max}^{scl} is associated with higher $g_{f_{D_1}}$ and vice versa. The figure also shows that $\sigma_{max}^{scl,V}$ and $\sigma_{max}^{scl,A}$ have a very similar behavior.
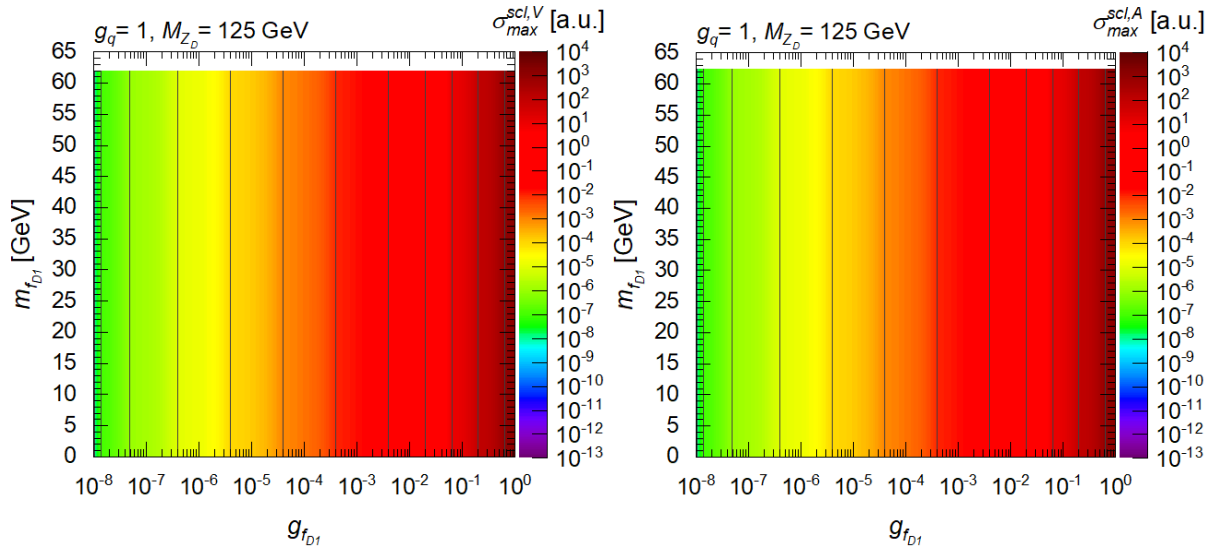
Figure 34: Variation of $\sigma_{max}^{scl,V}$ (left panel) and $\sigma_{max}^{scl,A}$ (right panel) in a scan over the $g_{f_{D_1}}$-$m_{f_{D_1}}$ plane for $g_q = 1$ and $M_{Z_D} = 125$ GeV.

9   Absolute production cross section of the dark vector boson

This section is a continuation of Sec. 4.2. Figure 35 is similar to Fig. 26 except that Fig. 35 is an implementation of another direct model [10] for Z_D set to have both vector and axial-vector couplings added. This assumption results in a similar behaviour of the simulated $\sigma(pp \to Z_D)$ against the analytical $c\tau_{max}^{V+A}$. The contribution of an axial-vector coupling to $\sigma(pp \to Z_D)$ is found to be negligible when added to that of a vector Z_D.
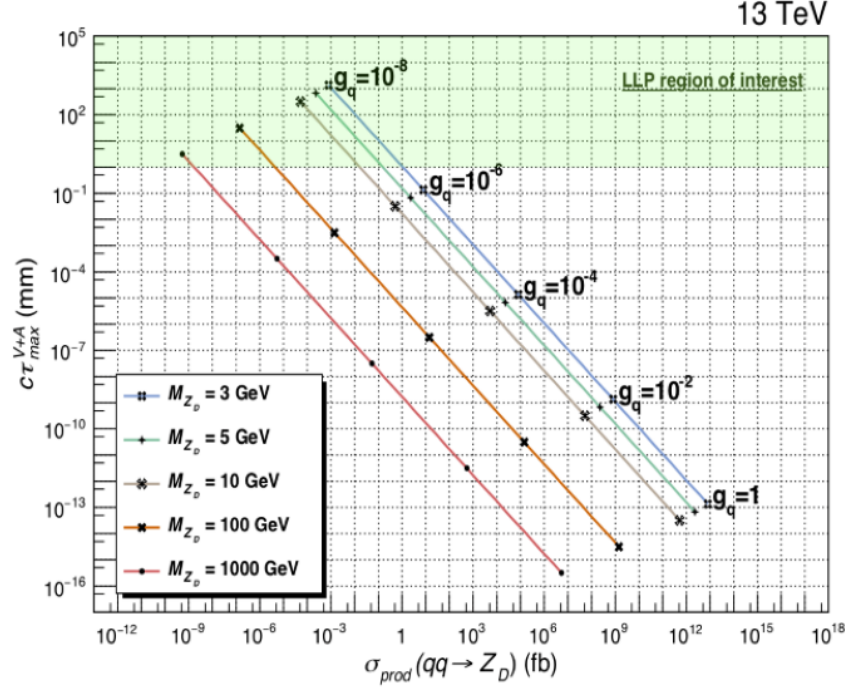
Figure 35: Two overlapped 1-dimensional plots showing how the MC simulated production cross section $\sigma(pp \to Z_D)$ and the analytically calculated $c\tau_{max}^V$ of a vector Z_D vary against each other for various values of g_q (joined points) and M_{Z_D} (separated points) and Run 2 of the LHC. Z_D for this plot is set to have both vector and axial-vector couplings to quarks.